Two-dimensional charge densities in intense rectangular ion beams with space-charge neutralization

Douglas A. Brown* and John F. O'Hanlon
Department of Electrical and Computer Engineering, University of Arizona, Tucson, Arizona 85721
(Received 16 August 1993; revised manuscript received 6 February 1995)

The physics of an intense (current density $\gtrsim 1$ mA/cm^2), positively charged, high aspect ratio rectangular ion beam is explored theoretically in a beam plasma containing a large density of space-charge neutralizing electrons. Before entering the plasma, the beam traverses an electron-free drift region in which it rapidly expands due to the mutual interion Coulomb repulsion. Within the beam plasma, the divergence rate is arrested by electron screening. Residual transverse velocities are small compared to the beam velocity and the beam ion density profile at the drift-plasma interface can be taken as longitudinally constant throughout the beam plasma. It is assumed that collisions between beam ions and residual gas molecules, producing a steady generation of electrons and slow residual gas ions, is the dominant mechanism sustaining the beam plasma. The cross-sectional profile of the beam ion distribution is of known form. To obtain the electron and slow-ion densities, charge is conserved and the energy balance of the plasma examined. Electron, slow-ion, and beam ion densities are then introduced into the two-dimensional Poisson equation to produce a second order partial integrodifferential equation requiring a numerical solution. This solution is obtained by expanding the density and potential functions in a complete set of orthogonal (Chebyshev) functions and reducing the differential equation to a system of linear algebraic equations. Applying the theory to a 100 keV, 10 mA, high aspect ratio arsenic beam, the electron density profile is predicted to display a shape similar to that of the beam ions. As with previous results for cylindrical beams, both the slow-ion and electron densities and, hence, the degree of space-charge neutralization are shown to depend strongly on the residual gas density, with the beam potential and electric field decreasing with increasing residual gas density. Unique to this analysis, it is predicted that the beam potential possesses substantial cylindrical symmetry even for very high aspect ratio rectangular beams, in complete agreement with recent experimental observations.

PACS number(s): 41.75.Ak, 41.85.Ew, 41.85.Ja

I. INTRODUCTION

Ever increasing use of high current, high aspect ratio rectangular ion beams in industrial and scientific applications has elevated the importance of developing a rigorous understanding of the fundamental principles of the formation, neutralization, and propagation of noncylindrical beams. This work addresses these issues for a rectangular beam, and provides the framework necessary to predict the beam profile, potential, and electric field under a variety of conditions.

Figure 1 displays a schematic representation of the beam under consideration. As shown, the beam system is comprised of four distinct segments: the *plasma source, drift region, beam plasma,* and the *sheath* at the beam-target interface. The beam itself is comprised of positive, nonrelativistic ions extracted continuously from the source, and provides a steady current to the target.

Ions in the source, with characteristic thermal energies of approximately 1–2 eV, are extracted and accelerated by the large potential difference between the source and beam line. Electrons emerging with the beam are reflected back into the source plasma by the electron suppression electrode, which also serves to confine beam electrons to the beam plasma and maintain an electron-free drift region. Passing through this electrode, the ions are shaped into a narrow charge configuration of nearly uniform density and well-defined aspect ratio. Upon entering the drift region, the beam begins to expand as the ions respond to their mutual Coulomb repulsion [1]. When controlled, this expansion produces a broad beam of longitudinally constant, nonuniform cross section, but if left unabated leads to overly divergent ion trajectories, degradation of beam definition, and beam stalling.

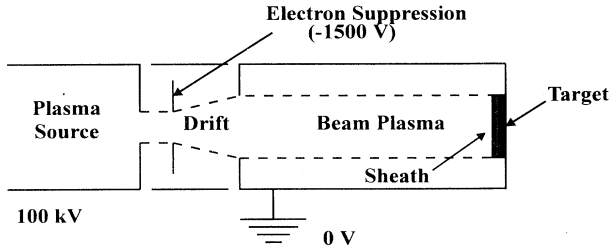

FIG. 1. Schematic representation of the beam under study. The beam is comprised of four distinct regions: the plasma source, the extraction and drift region, the beam plasma, and the sheath at the beam-target interface.

*Present address: Varian Ion Implant Systems, Gloucester, MA, 01930-2297.

In the beam plasma, divergence is arrested by the charge screening effect of an electron swarm. Electrons liberated by ionizing collisions of beam ions with residual gas molecules, and secondary emission from the target and apertures, engulf the beam and neutralize its space-charge potential. Upon entering the beam plasma, maximum transverse velocities are on the order of 10^2 m/s as compared to the longitudinal velocity, $v_b \sim 10^5$ m/s. Thus, for beamlines on the order of 1 m in length, the beam's shape, as it enters the beam plasma, is essentially retained along the remainder of its path, rendering the beam divergence negligible within the beamline.

In the steady state, the beam plasma is sustained by a constant creation of charge. Slow ions are continuously produced from residual gas molecules as they interact with the beam in ionizing and charge exchanging events. Electrons produced by ionization of gas molecules quickly thermalize, with the higher energy electrons flowing steadily out of the beam. These mechanisms create a balance in which the net charge in the beam region is slightly positive. Lower energy electrons are confined by this net potential, but collisions continuously excite some electrons to energies in excess of the beam potential. These higher energy electrons escape from the beam, producing a current that exactly offsets the electron creation rate and maintains a steady-state electron distribution. Due to the net positive charge in the vicinity of the beam, slow ions are also expelled at a constant rate equal to their rate of generation.

At the beam-target interface, a plasma sheath arises from the potential difference between the beam and the target. Electrons in the swarm neutralizing the beam's space charge have no preferred direction of propagation, their velocities being randomized by thermalizing processes. Therefore the beam potential, which is more positive than that of the target, can confine most of the electrons, permitting only the higher energy negative charge carriers to reach the target. The energy spectrum of electrons penetrating the sheath depends on the electric field between the beam plasma and the target's surface. In turn, this field varies with target composition and topology. Since the beam potential results from the delicate balance of charge creation and escape rates, perturbations in the electron and slow-ion currents at the sheath are expected to affect the net charge density and potential of the beam. However, as with stationary plasmas, the perturbation will have a characteristic length scale on the order of the Debye length and will not affect the principal processes occurring within the bulk of the beam.

As a follow-up to the authors' previous work, in which an unneutralized beam was analyzed and the properties of the beam within the drift region determined [1], this study examines a quasineutral beam as it propagates, and investigates the mechanisms sustaining a steady-state plasma in the beamline. Initial charge densities and potentials are calculated in the drift region and used as the initial condition for the ion configuration as the beam enters the neutralized plasma. Inside the beam plasma, physical processes are described mathematically, and the density and potential calculated under the assumption that the target and apertures are sufficiently far removed such that interactions maintaining the charge distributions are dominated by local ionization and charge exchanging events. A technique for numerically integrating the resulting partial integrodifferential equation is implemented [2], and theoretical predictions of beam potentials, electron temperatures, and ion densities presented.

II. THE BEAM PLASMA

A self-consistent description is formulated for a rectangular beam plasma comprised of four types of charge carriers: beam ions, slow residual gas ions, electrons confined by the beam's net positive potential relative to the chamber walls, and fast electrons that escape from the beam. Initially, the potential distribution is treated as known, and the charge densities found as functions of this potential. Charge is conserved to determine the slow-ion density, while the electron density is obtained from solutions of the Fokker-Planck and velocity-space diffusion equations. Energy balance between the beam ions and the electron cloud is then considered to determine the electron temperature. The self-consistent description is completed by requiring the densities and potential to satisfy Poisson's equation. This results in a nonlinear partial integrodifferential equation requiring numerical solution.

A. The electron density

Unlike ions comprising the collisionless beam in the drift region, electrons in the beam plasma continuously experience energy and momentum transferring events. Free electrons engulfing the beam absorb energy from the beam ions, thermalize, and eventually evaporate from the beam as random collisions excite them to energy levels in excess of the beam potential. As these electrons escape, they are replaced by newly created electrons with near zero velocity [3,4]. In terms of the velocity-space distribution, there is a sharp peak at low velocities and a truncation velocity at the beam potential above which there are no electrons (Fig. 2). This situation leads to a steady-state system of time invariant charge density; however, the system is not in equilibrium. To determine the phase-space distribution function, and hence the configuration-space density, the full Boltzmann equation must be used. In general, this equation is difficult to solve, but it can often be transformed into the Fokker-Planck equation which is sometimes simpler to treat. Rosenbluth, MacDonald, and Judd have derived the Fokker-Planck equation for particles interacting through an inverse square force law [5]. Assuming an isotropic distribution, their result can be expressed in spherical coordinates, and is given by

$$\left[\frac{\partial f}{\partial t}\right]_c = \frac{\Gamma}{v^2}\left[-\frac{\partial}{\partial v}\left[fv^2\frac{\partial h}{\partial v}+f\frac{\partial g}{\partial v}\right] + \frac{1}{2}\frac{\partial^2}{\partial v^2}\left[fv^2\frac{\partial^2 g}{\partial v^2}\right]\right], \tag{1}$$

where, for scattering centers of mass m_i, with distributions f_i,

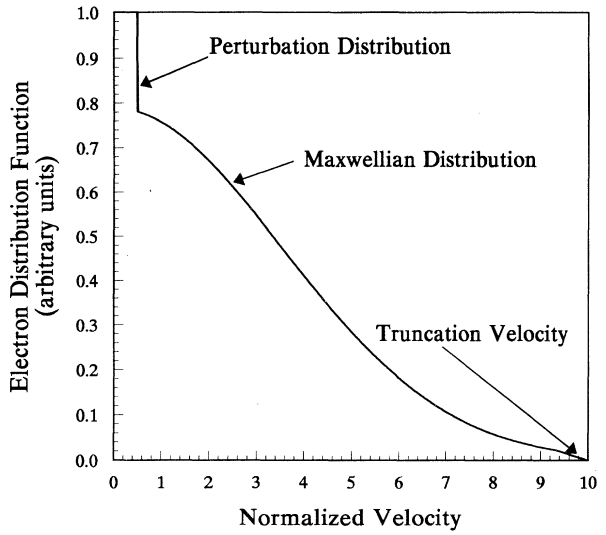

FIG. 2. Perturbed Maxwellian electron distribution. Overall, the electron distribution is assumed to be Maxwellian; however, there is a small contribution to the distribution arising from a spike at low velocities due to newly created electrons. The high energy tail is truncated at $v=\sqrt{2q\phi_0/m_e}$ ($=10$ in the arbitrary units defined here) by the finite beam potential.

$$\Gamma=\frac{4\pi q^2}{m_e^2}\lambda_d \ln(\tfrac{1}{2}\mu u^2) ,$$

$$h(v)=\sum_i \frac{m_e+m_i}{m_i}\left[\frac{4\pi}{v}\int_0^v f_i v'^2 dv'+4\pi\int_v^\infty f_i v' dv'\right] ,$$

$$g(v)=\sum_i \frac{4\pi}{3}\left[\frac{1}{v}\int_0^v f_i v'^2(3v^2+v'^2)dv' + \int_v^\infty f_i v'(3v'^2+v^2)dv'\right] .$$

The Debye length is denoted λ_d, and μ and u are the reduced mass and center of mass velocity, respectively, for the scatterers.

In general, it is impossible to solve Eq. (1) analytically. However, as can be shown by direct substitution, the Maxwell-Boltzmann distribution function is a stationary solution of Eq. (1). Thus it is possible to separate the distribution into a linear combination of the time independent Maxwellian and a perturbation describing the effects of electron creation. Experiments by Rudd and Jorgensen [3] and theoretical work by Gryzinski [4] have established that the majority of newly created electrons possess small initial velocities. Through thermalizing events, newly liberated electrons are rapidly absorbed into the Maxwellian distribution and are no longer part of the perturbation. Thus the perturbation may be considered as comprising an immobile ensemble of electrons with a density that is proportional to the creation rate at the point of interest [i.e., $\delta n_e(x,y)=n n_b(x,y) v_b \sigma_i \delta t$]. This perturbation is maintained by steady-state processes, but is established during the transient period after the electron cloud has been formed and prior to the onset of the steady state. An estimate of the upper limit to this relaxation time δt is presented in Appendix A. There, it is shown that δt scales approximately as $10^7/n_e$. Typical values of the perturbation parameters are $n\sim 10^{18}$ m^{-3} (residual gas density for a beamline pressure of approximately 10^{-6} Torr), $n_{b0}\sim n_{e0}\sim 10^{12}$–$10^{14}$ m^{-3} (axial beam and electron densities), $\sigma_i\sim 10^{-21}$ m^2 (cross section for ionization), and $v_b\sim 10^5$ m/s (beam velocity). These values produce an order of magnitude estimate, $\delta n_e\sim 10^9$ m^{-3}, which is negligible compared to the typical values of the electron density, n_e, within the beam. Thus, for the density calculation, the electron ensemble will be considered a truncated Maxwellian.

For stationary states, the equilibrium Boltzmann equation is applicable, and for the Maxwellian velocity distribution the corresponding density function, derivable from Eq. (1), is the standard Maxwell-Boltzmann distribution for a system in a conservative energy field. Properly normalized to account for the spatial dependence of the truncation velocity it takes the form

$$n_e(x,y)=n_{e0}\frac{\int_0^v e^{-mv'^2/2kT}d^3v'}{\int_0^{v_{\max}} e^{-mv'^2/2kT}d^3v'} , \tag{2}$$

where $v=\sqrt{2q[\phi_0+\phi(x,y)]/m_e}$ and $v_{\max}=\sqrt{2q\phi_0/m_e}$ are the escape (truncation) velocities at (x,y) and (0,0), respectively. The potential is defined to be zero along the beam axis, decreasing to a minimum, $-\phi_0$, at the walls.

As shown in Appendix B, both the numerator and denominator can be integrated in two separate ways; yielding functionally different, but equivalent results.

$$\frac{n_e(x,y)}{n_{e0}}=\frac{(\sqrt{\pi}/2)e^{(q/kT)(\phi_0+\phi)}\mathrm{erf}[\sqrt{(q/kT)(\phi_0+\phi)}]-\sqrt{(q/kT)(\phi_0+\phi)}}{(\sqrt{\pi}/2)e^{q\phi_0/kT}\mathrm{erf}(\sqrt{q\phi_0/kT})-\sqrt{q\phi_0/kT}} , \tag{3}$$

$$\frac{n_e(x,y)}{n_{e0}}=\frac{e^{q\phi/kT}\left[(q/kT)(\phi_0+\phi)\mathrm{erf}[\sqrt{(q/kT)(\phi_0+\phi)}]-\int_0^{\sqrt{(q/kT)(\phi_0+\phi)}}\mathrm{erf}(u)2u\,du\right]}{(q\phi_0/kT)\mathrm{erf}(q\phi_0/kT)-\int_0^{\sqrt{q\phi_0/kT}}\mathrm{erf}(u)2u\,du} . \tag{4}$$

Equation (3) is useful in verifying the asymptotic behavior of the distribution, while Eq. (4) is valuable in generating a more convenient function approximating the density.

Consider first the limiting case of infinite plasma potential, $\phi_0 \rightarrow \infty$. This corresponds to a fully confined system. From Eq. (3), in this limit, the standard Maxwell-Boltzmann distribution is recovered.

$$\lim_{\phi_0 \rightarrow \infty} n_e(x,y) = n_{e0} \frac{(\sqrt{\pi}/4) e^{(q/kT)(\phi_0+\phi)}}{(\sqrt{\pi}/4) e^{(q/kT)\phi_0}} = n_{e0} e^{q\phi/kT} .$$

By inspection of Eq. (3), it is also evident that as $\phi \rightarrow -\phi_0$ the electron density vanishes, as it must since the potential approaches this limit far from the beam's axis where charge carriers are nonexistent.

Observe that these two limiting properties are also manifest in Eq. (4), even when the integrals in the numerator and denominator are both neglected. Moreover, the error functions of square roots vary slowly with their arguments, and the ratio

$$\text{erf}[\sqrt{q(\phi_0+\phi)/kT}\,]/\text{erf}[\sqrt{q\phi_0/kT}\,]$$

is a slowly varying function of order unity. This suggests the use of an approximation free of the complicated error function. Neglecting the integrals, and canceling the error functions, Eq. (4) assumes the much simpler form

$$n_e(x,y) \cong n_{c0} \left[\frac{\phi_0+\phi}{\phi_0} \right] e^{q\phi/kT} . \quad (5)$$

Comparison of the plots in Fig. 3 graphically illustrates the close agreement between approximation (5) and Eqs. (3) and (4).

It remains to determine n_{e0}, the electron density along the axis of the beam. However, this requires additional information and will be deferred until the relation describing the slow-ion density has been obtained.

B. Slow-ion density

Residual gas molecules, continuously ionized by Coulomb interactions with beam ions, become slow, low energy ions that give rise to a constant positively charged particle flux emanating from the beam. To determine the density of these slow ions at any point in space, a differential form of the continuity equation is employed to conserve mass.

As depicted in Fig. 4, slow ions created at (x_0,y_0) are expelled outward. Since the thermal energy of the residual gas is small ($\sim$0.025 eV) compared to the energy of slow ions falling through the potential well ($\sim$1–100 eV), slow-ion motion may be considered field dominated. These ions will then follow a trajectory $f(x)$ that traces the electric field lines from the point of ion creation to final expulsion from the beam. Along this trajectory, they contribute to the particle flux through any surface parallel to the y-z plane. To conserve this slow-ion flux, the creation rate of slow ions at (x_0,y_0) is related to the flux at (x,y), through the equation of continuity:

$$n n_b(x_0,y_0)\sigma_t v_b dx_0 dy_0 dz = dn_i(x,y) v \cos\theta \, dy \, dz . \quad (6)$$

σ_t is the total cross section for charge exchange and ionization, v_b is the beam velocity, and

$$v = \sqrt{2q[\phi(x_0,y_0)-\phi(x,y)]/m_i}$$

is the slow-ion velocity produced from acceleration by the electric field. From the simple geometry $dy = dy_0$, and from elementary calculus

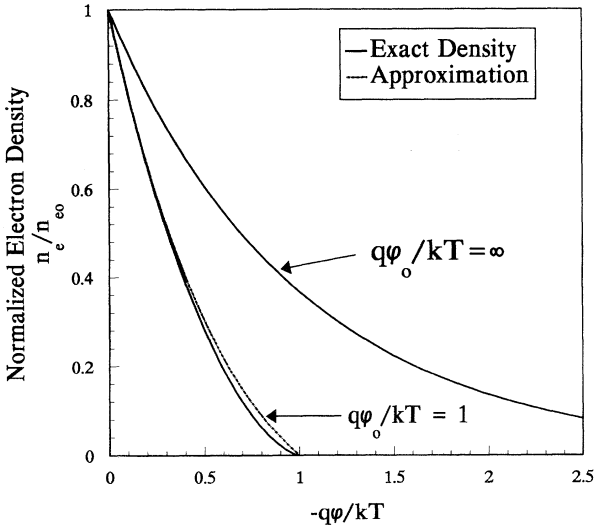

FIG. 3. Comparison of the exact and approximate electron densities. Computations were performed with $kT = q\phi_0$, since this is the value of the electron temperature predicted by the theory. In the limit $q\phi_0/kT \rightarrow \infty$, the system is fully confined and the Maxwell-Boltzmann distribution is recovered.

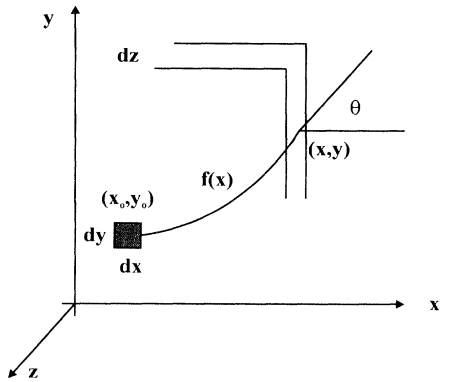

FIG. 4. Slow ions, created with low velocity at the point (x_0,y_0), follow trajectories $f(x)$ defined by the electric field lines and contribute to the particle flux through a surface at (x,y). The slow-ion density at the point (x,y) is found by integrating the contributions from all volumetric elements with trajectories passing through the point (x,y).

$$\cos\theta = dx/\sqrt{dx^2+dy^2} = 1/\sqrt{1+[f'(x)]^2} .$$

Thus, if $y=f(x)$ is a known trajectory, the slow-ion density can be found by integrating Eq. (6) over all points $[x_0, f(x_0)]$, $x_0 \le x$, with trajectories passing through the point (x,y). Solving for dn_i and integrating yields

$$n_i(x,y) = n\sigma_t v_b \sqrt{1+[f'(x)]^2} \left[\frac{m_i}{2q}\right]^{1/2} \times \int_0^x \frac{n_b[x_0, f(x_0)]dx_0}{\sqrt{\phi[x_0, f(x_0)]-\phi(x,y)}} . \quad (7)$$

The shape of the potential well can be inferred from Eq. (7). Along the beam's axis, the slow-ion density must be nonvanishing and finite. It is shown by Holmes [6] and demonstrated in Appendix C, that the only potential consistent with a finite axial slow-ion density is parabolic. With this form of the potential, the axial density is determined to be

$$n_{i0} = v_b n n_{b0} \sigma_t r_0 \left[\frac{3m_i}{2q\phi_0}\right]^{1/2} , \quad (8)$$

where r_0 is a characteristic length scale for the potential. In general, r_0 is unknown, but may be found from the charge neutrality condition, $n_{e0} = n_{i0} + n_{b0}$.

C. n_{e0}, ϕ_0, and kT

Equation (5) is the preferred representation of the electron density. However, n_{e0}, ϕ_0, and kT remain undetermined. To calculate these quantities, it is necessary to derive an expression for the electron density, which for a rectangular beam is valid only in the very close vicinity of the beam's central axis. In this section, the electron density in configuration space is calculated by solving the velocity-space diffusion equation. In cylindrical coordinates, this equation assumes a form that is soluble by direct integration. Cylindrically symmetric forms of the ion density and potential are therefore assumed and this interim analysis confined to a narrow region about the central axis of the beam. In generating these symmetric functions, two new parameters are introduced which are ultimately used to produce algebraic equations that uniquely determine the value of n_{e0}, ϕ_0, and the electron temperature kT. The basic approach, similar to that proposed by Holmes in his study of a cylindrical ion beam [6], is valid because, as previously shown [1], in the limit of vanishing x and y the ion density possesses a high degree of cylindrical symmetry.

Along the axis, the beam ion density will be assumed to be a simple Gaussian profile with a characteristic dimension r_0 [1,6]:

$$n_b(x,y) \cong n(r) = n_{b0} e^{-(r/r_0)^2} . \quad (9)$$

In the subsequent development, the use of a simple parabolic potential, as required for a finite slow-ion density, leads to intractable expressions for the sought variables. However, invoking the constraint $r/r_0 \ll 1$, the potential can be taken as exponential:

$$\phi(x,y) \cong \phi(r) = -\phi_0 \beta^2 \frac{r^2}{r_0^2} \cong -\phi_0 (1 - e^{-\beta^2 (r/r_0)^2}) . \quad (10)$$

This relation will be rigorously true in the limit of vanishing r.

In the steady state, newly created electrons must diffuse outward against the confining potential and eventually evaporate from the plasma. As an electron migrates further from the axis, the depth of the potential well diminishes, and the increment of velocity needed to escape is reduced. In this way, the scalar potential uniquely couples the velocity-space and configuration-space coordinates. In particular, if $v(r)$ is the escape velocity at the point r, then the isomorphic transformation mapping the two spaces is $v = \sqrt{2q[\phi_0 + \phi(r)]/m_e}$. Utilizing this fact, the densities in each of the coordinate systems can be related.

Let $n_v(v)$ be the number of electrons with velocities between v and $v+dv$ and $n_e(r)$ be the number of electrons between r and $r+dr$. Then, in cylindrical coordinates,

$$2\pi n_v v\, dv = 2\pi n_e r\, dr .$$

The coordinate transformation is such that increasing v corresponds to decreasing r. Thus the derivatives dr/dv and dv/dr are inherently negative. Inserting a minus sign to maintain a positive density, n_v is related to n_e by

$$n_v = -n_e \frac{r}{v}\frac{dr}{dv} . \quad (11)$$

Diffusion in velocity space is governed by the equation

$$\frac{\partial n_v}{\partial t} = \nabla\cdot(D_v \nabla n_v) ,$$
$$D_v = \left[\frac{0.97 q^4 \ln\Lambda}{2\pi\epsilon_0^2 m^2}\left[\frac{m}{2kT}\right]^{1/2}\right] n_e \equiv C n_e . \quad (12)$$

The diffusion coefficient D_v is the velocity dispersion coefficient calculated by Spitzer [7] for an electron gas. The term Λ is a characteristic value of a plasma, defined as the ratio of the Debye length to the two-body impact parameter. Its precise value depends on the density and temperature of the electrons, with $\ln\Lambda$ ranging in value from about 6 to 35 [7]. Conventionally, $\ln\Lambda$ is taken to be 10 [7].

The partial time derivative of the electron density in real space is equal to the electron creation rate. If n is the residual gas density and σ_i the cross section for ionization, the time derivative of n_e can be expressed in terms of the collision rate between gas molecules and beam ions:

$$\frac{\partial n_e}{\partial t} = n n_b \sigma_i v_b .$$

Thus the partial time derivative of n_v may be written

$$\frac{\partial n_v}{\partial t} = -n n_b \sigma_i v_b \frac{r}{v}\frac{dr}{dv} . \quad (13)$$

Using Eq. (13) for the time derivative of n_v and ex-

panding the divergence term in cylindrical coordinates, the diffusion relation, Eq. (12), for a beam with axial and azimuthal symmetry becomes

$$\frac{1}{v}\frac{d}{dv}\left[vD_v\frac{dn_v}{dv}\right]=-nn_b\sigma_i v_b\frac{r}{v}\frac{dr}{dv}\ . \tag{14}$$

Rearranging terms, Eq. (14) can be immediately integrated to yield

$$vCn_e\frac{dn_v}{dv}=\frac{n\sigma_i v_b r_0^2 n_{b0}}{2}e^{-(r/r_0)^2}+c_1\ , \tag{15}$$

where the diffusion coefficient has been replaced by its functional value, and Eq. (9) has been used for the beam ion density. Both n_e and n_v vanish at large r; so the constant of integration c_1 is zero.

Equation (11) also provides n_e in terms of n_v which permits Eq. (15) to be rewritten as

$$Cv^2 n_v\frac{dv}{dr}\frac{dn_v}{dn}=-\frac{n\sigma_i v_b r_0^2 n_{b0}}{2}e^{-(r/r_0)^2}r\ .$$

Using

$$\begin{aligned} dv&=-\beta^2\left[\frac{2q\phi_0}{m_e}\right]^{1/2}\frac{r}{r_0^2}e^{-(1/2)(\beta r/r_0)^2}dr\ ,\\ v^2&=\frac{2q\phi_0}{m_e}e^{(\beta r/r_0)^2}\end{aligned} \tag{16}$$

and rearranging the differentials, the velocity-space diffusion relation is again integrable:

$$Cn_v dn_v=-\frac{nn_{b0}\sigma_i v_b m_e r_0^2}{4q\phi_0}re^{-(1-\beta^2)(r/r_0)^2}\ .$$

Performing the integration yields an expression in n_v^2,

$$n_v^2=\frac{1}{C}\frac{m_e}{4q\phi_0}\left[\frac{nn_{b0}\sigma_i v_b r_0^4}{1-\beta^2}\right]e^{-(1-\beta^2)(r/r_0)^2}+c_2\ . \tag{17}$$

Again, the density must vanish at larger r, and it may be concluded that $0\le\beta^2<1$ and $c_2=0$.

Employing Eqs. (11) and (16) and using the value of C from Eq. (12), Eq. (17) can be rewritten to obtain the final expression for the electron density:

$$\begin{aligned} n_e(r)&=n_{e0}e^{-(1/2)(1+\beta^2)(r/r_0)^2}\ ,\\ n_{e0}&=\left[\frac{2\pi nn_{b0}\sigma_i v_b m_e\epsilon_0^2\beta^4\phi_0}{0.97q^3(1-\beta^2)\ln\Lambda}\left[\frac{2kT}{m_e}\right]^{1/2}\right]^{1/2}\ .\end{aligned} \tag{18}$$

To determine the value of the unknown parameter β^2, an equation or system of equations with a unique solution must be derived. Since this parameter appears only in expressions for the electron density, ion density, and potential, a relationship involving these quantities must be developed. To accomplish this, the energy balance of the beam-electron system will be explored.

Propagating down the beamline, the beam ions transport kinetic energy into every volumetric element of the beam. A portion of this energy is continuously imparted to the electron cloud. Under steady-state conditions, this energy is then removed from the electron distribution by high energy electrons evaporating from the beam. These escaping particles carry away essentially no kinetic energy, for they escape just as they have attained the escape velocity. Thus the rate of energy absorption into the electron distribution must equal the rate per unit volume at which electrons surrender kinetic energy to the electric field. Energy transfer may therefore be considered a three-step process. At any point in the beam, energetic beam ions interact through the Coulomb force to excite electrons to higher energy states. These excited electrons then expand outward, storing energy in the beam's electric field. This stored energy is then returned to the distribution by accelerating some electrons towards the high energy tail of the distribution, and is ultimately lost to electrons attaining the truncation energy.

In any given volume element within the beam, it will be assumed that the imparted beam energy is shared uniformly among the electrons. Denoting the electron potential energy per unit volume by U, the rate at which electrons at the point r expend kinetic energy by advancing against the electric field is given by

$$\begin{aligned}\frac{dU}{dt}&=-qv_e(r)n_e(r)\frac{d\phi}{dr}\\ &=2qv_e(r)n_e(r)\phi_0\beta^2\frac{r}{r_0^2}e^{-\beta^2(r/r_0)^2}\ ,\end{aligned} \tag{19}$$

where Eq. (10) was used to obtain the last line and v_e is a characteristic velocity.

At every point within the beam, newly created electrons replace escaping Maxwellian electrons in such a way that the density $n_e(r)$ is constant in time. The fractional creation rate of electrons, defined to be the rate of creation at r divided by the number density at r, provides a characteristic time scale for the motion of electrons emanating from a given point inside the beam. Thus, if some length scale, r_0 for example, could be ascribed to the system, then electron motion could be characterized by a radial velocity

$$v_e(r)=\frac{n\sigma_i v_b n_b(r)}{n_e(r)}r_0\ .$$

The actual value of v_e is unimportant. For the energy balance analysis, the critical feature is that v_e scales as n_b/n_e. Substituting this value of the characteristic velocity into Eq. (19), the radial energy transfer rate for electrons becomes

$$\frac{dU}{dt}=2qn\sigma_i v_b n_{b0}\phi_0\beta^2\frac{r}{r_0}e^{-(1+\beta^2)(r/r_0)^2}\ . \tag{20}$$

In the steady state, the electron temperature and the beam's electric field are both constant. Thus, at any point r, the rate at which the electron distribution absorbs energy must equal the rate at which kinetic energy is converted to potential energy stored in the field, before being ultimately lost to the evaporating electrons. If α is the total fraction of the beam's kinetic energy absorbed by the distribution at r, and $dE(r)$ is the newly acquired electron kinetic energy per unit length at r, then

$$dE(r)=\alpha\tfrac{1}{2}m_b v_b^2 n_b(r)(2\pi r dr) .$$

Multiplying this expression by the characteristic energy flux velocity, which scales as rv_e/r_0, and introducing a new constant prefactor α', the rate of energy absorption by electrons in an annulus of thickness dr and radius r can be expressed

$$v_e(r)\frac{r}{r_0}dE(r) = \alpha'\pi m_b v_b^3 n\sigma_i \frac{n_{b0}^2}{n_{e0}}\frac{r^2}{r_0^2}e^{-(1/2)(3-\beta^2)(r/r_0)^2}dr .$$

If the annulus displaces a volume $dV(=2\pi z' r dr)$, then $dV(dU/dt)=rv_e dE/r_0$, and energy conservation requires

$$4\pi z' q n\sigma_i v_b n_{b0}\phi_0\beta^2\frac{r^2}{r_0}e^{-(1+\beta^2)(r/r_0)^2}dr = \alpha'\pi m_b v_b^3 n\sigma_i \frac{n_{b0}^2}{n_{e0}}\frac{r^2}{r_0^2}e^{-(1/2)(3-\beta^2)(r/r_0)^2}dr . \quad (21)$$

For Eq. (21) to be true, the functional dependencies must be the same on each side of the equation. In particular, the values of the exponents must be equal. Equating these exponents, the value of the sought parameter is obtained.

$$-(1+\beta^2)=-(1/2)(3-\beta^2) , \quad \beta^2=\tfrac{1}{3} . \quad (22)$$

With the value of β^2 known, it is now possible to relate the electron temperature to the beam potential ϕ_0. Since the velocity distribution is assumed to be Maxwellian, the number of electrons with escape velocities in a velocity-space volume about the point $\mathbf{v}$ is given by a function of the form

$$f(v)=Ne^{-mv^2/2kT} .$$

Using the escape velocity $v(r)=\sqrt{2q[\phi_0+\phi(r)]/m_e}$, which in the cylindrically symmetric approximation is

$$v(r)=\sqrt{2q\phi_0/m_e}\exp[-\tfrac{1}{2}\beta^2(r/r_0)^2] ,$$

the function f may be written

$$f(v)=f(r)=Ne^{-(q\phi_0/kT)\beta^2(r/r_0)^2} .$$

This expression must equal the value of n_v from Eq. (17). Again, the exponents must be equal:

$$-\beta^2\frac{q\phi_0}{kT}\left[\frac{r}{r_0}\right]^2=-\frac{(1-\beta^2)}{2}\left[\frac{r}{r_0}\right]^2 .$$

Setting $\beta^2=\frac{1}{3}$, the electron temperature is immediately obtained:

$$kT=q\phi_0 . \quad (23)$$

Although this value of the electron temperature was acquired along the axis of the beam, it is valid throughout the electron distribution, for there are no temperature gradients. As known from kinetic theory, an equilibrated system in a conservative force field displays a uniform temperature [8].

Finally, to complete the description of the beam plasma near the central axis, axial charge neutrality will be invoked to determine the beam potential. Referring to Eqs. (8) and (18), the charge neutrality condition, $n_{e0}=n_{i0}+n_{b0}$, may be expressed

$$n_{e0}=\left[\frac{2\pi n n_{b0}\sigma_i v_b m_e\epsilon_0^2\beta^4\phi_0}{0.97q^3\ln\Lambda(1-\beta^2)}\left[\frac{2kT}{m_e}\right]^{1/2}\right]^{1/2} = \left[1+v_b n\sigma_t r_0\left[\frac{3m_i}{2q\phi_0}\right]^{1/2}\right]n_{b0} .$$

At beamline pressures below about 0.1 mTorr, the residual gas density is sufficiently low that the term involving n on the right hand side is small compared to unity, and $n_{e0}\approx n_{b0}$. Substituting the known values for β^2 and kT, the beam potential is found to be

$$\phi_0\cong\left[\frac{2.06q^3\ln\Lambda}{\pi\sigma_i v_b(qm_e)^{1/2}\epsilon_0^2}\left[\frac{n_{b0}}{n}\right]\right]^{2/3} . \quad (24)$$

With the inclusion of the beam potential ϕ_0, all of the unknown parameters necessary for a complete description of the beam (i.e., ϕ_0, kT, n_{e0}, and n_{i0}) have been determined.

III. THE BEAM PLASMA EQUATION

Returning to the unsimplified case of a fully rectangular beam, each of the densities is a function of the unknown potential $\phi(x,y)$. To complete the self-consistent picture of the beam plasma, these densities must satisfy Poisson's equation:

$$\nabla^2\phi(x,y)=-\frac{q}{\epsilon_0}[n_b(x,y)+n_i(x,y)-n_e(x,y)] , \quad (25)$$

where the beam ion density is given by [1]

$$n_b(x,y)=\left[1-\frac{1}{\eta^2}\right]\frac{\epsilon_0}{q}\sum_{m,n=0}^{\infty}a_{mn}\gamma_{nm}^2\cos(\alpha_n x)\times\cos(\beta_m y)e^{-(\gamma_{nm}/\eta)z_0} ,$$

$$\alpha_n=\frac{(2n+1)\pi}{2L_x} ,$$

$$\beta_m=\frac{(2m+1)\pi}{2L_y} ,$$

$$\gamma_{nm}=\frac{\pi}{2}\left[\left[\frac{2n+1}{L_x}\right]^2+\left[\frac{2m+1}{L_y}\right]^2\right]^{1/2} ,$$

z_0 is the length of the drift region, L_x and L_y are the distances from the center of the beam to the walls, and $\eta^2=1+v_z\sqrt{2m_b/kT_b}$. The electron and slow-ion densities are given by Eqs. (5) and (7), respectively.

Poisson's equation, together with these densities, comprises the beam plasma equation. Neither the slow-ion trajectory $f(x)$ nor $\phi(x,y)$ are known. However, $f(x)$ is assumed to trace the gradient of ϕ and the differential equation is not underdetermined. Still, a sin-

gle solution is not adequate and a relaxation routine must be incorporated into the numerical algorithm.

IV. DISCUSSION AND RESULTS

Implementing a numerical algorithm utilizing Chebyshev polynomials [2], charge density and potential profiles were calculated for a 100 keV, 10 mA beam at chamber pressures of 5×10^{-6} and 5×10^{-3} Torr. To amplify the space-charge effects under study, arsenic was chosen as the beam species for its large mass, and subsequent lower velocity (hence, greater beam ion density) at any given beam energy and current. The results are presented graphically in Figs. 5–12. As indicated by Eqs. (8) and (18), the slow-ion and electron densities rise with increasing residual gas density n. Since the slow ions are expelled while the electrons are attracted towards the center of the beam, the theory predicts greater space-charge neutralization and reduced beam potentials at higher residual gas densities. Moreover, it is predicted that even for a high aspect ratio beam the potential will retain significant cylindrical symmetry, a prediction which is in excellent agreement with recent experimental observations utilizing rectangular beams [9].

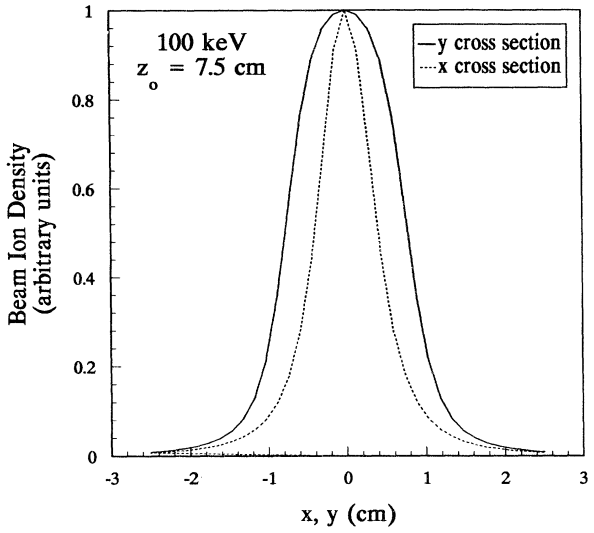

FIG. 6. x and y cross sections of the arsenic beam ion profile. Defining the beam width as the distance between the points of half maximum, this beam has an aspect ratio of approximately 2:1.

100 keV, 10 mA arsenic beam

The drift region length for the 100 keV, 10 mA, arsenic beam was set at 7.5 cm from an emission aperture 1.5 cm high and 0.5 cm wide. Figures 5 and 6 display the resulting normalized beam ion density. Defining the beam width as the distance between the points of half maximum, the final cross section is approximately 1.6×0.8 cm^2. This profile is assumed constant throughout the beam plasma, and is independent of beamline pressure.

At a pressure of 5×10^{-6} Torr, the electron density assumes the profile presented in Figs. 7 and 8. In performing this calculation, charge neutrality was initially demanded along the central axis. Then, as the system began to converge, this requirement was relaxed and the axial potential and densities determined self-consistently. It can be seen in Fig. 8 that along the beam axis the electron density is predicted to be approximately 6% less than that of the beam ions. Moreover, the slow ions contribute nearly an additional 6% to the positive charge density. Since this analysis treats the electrons as instantaneously thermalizing upon liberation, the electron density profile represents a condition of thermal equilibrium balancing the electron creation rate, escape rate, and final

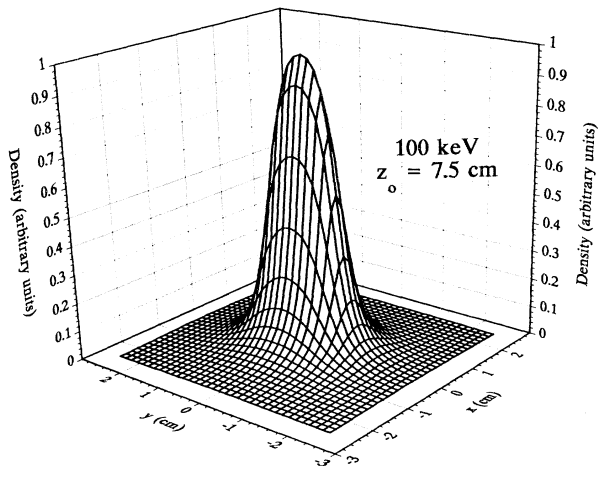

FIG. 5. Beam ion density profile for a 100 keV, 10 mA arsenic beam as the beam enters the beam plasma a distance $z_0=7.5$ cm from the electron suppression electrode. Further beam expansion is neglected and this profile is assumed throughout the plasma region.

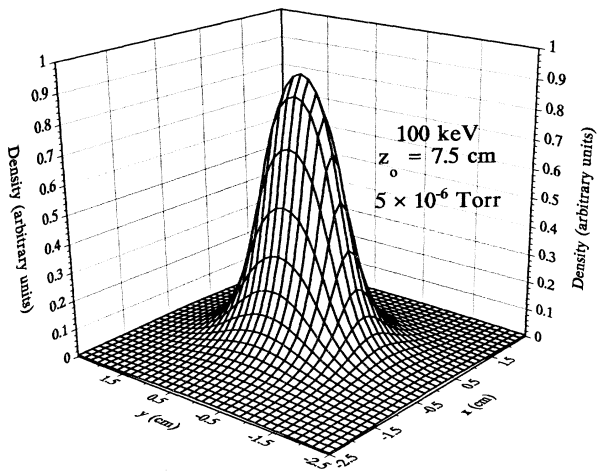

FIG. 7. Electron density within the beam plasma for a beam with a 7.5 cm drift region, and beamline pressures of 5×10^{-6} Torr.

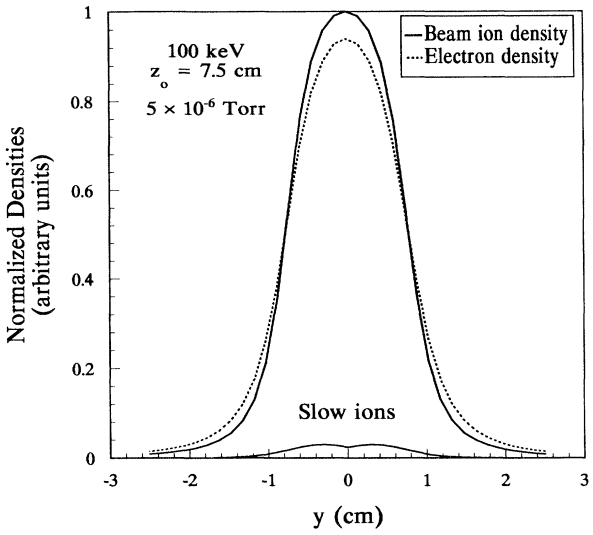

FIG. 8. Beam ion, slow-ion, and electron density y-axis cross sections for a 100 keV, 10 mA arsenic beam. At 5×10^{-6} Torr, neutralization is incomplete and the positive ion density exceeds that of the electrons along the axis.

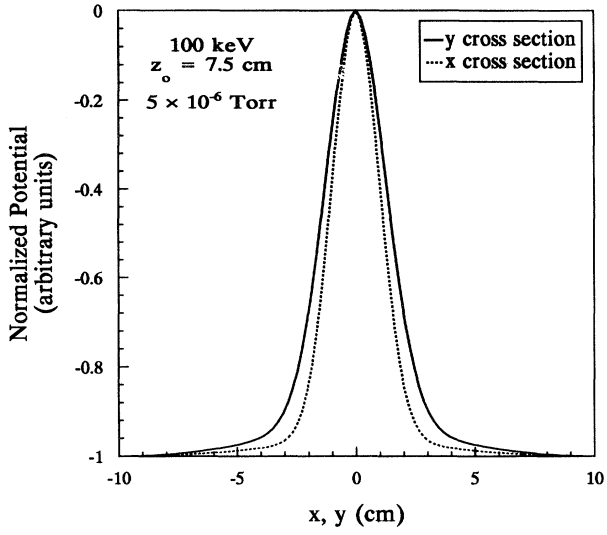

FIG. 10. x and y cross sections of the potential for a 100 keV, 10 mA arsenic beam. The small aspect ratio is apparent from the widths of the two plots.

beam potential (electron temperature). At this pressure, the electron creation rate is low, resulting in a beam that is only partially neutralized, with a substantial net positive core.

Within the beam, the resulting potential profile (Figs. 9 and 10) displays a well-defined aspect ratio, but possesses considerably more cylindrical symmetry than the charge density distributions. At the periphery, the potential presents the greatest asymmetry, decaying more slowly along the coordinate axes than along any of the diagonals in the x-y plane. Comparison to the potentials predicted for the unneutralized beams [1] reveals that space-charge neutralization produces a broader, more slowly varying profile along the central axis, but also reduces the spatial extent of variations in the potential. The potential gradients are steeper near the periphery than in the unneutralized case; however, the electric field is weaker as the beam potential ϕ_0 is more than an order of magnitude lower than the beam potential in the drift region. (Typical values for the potential, given a beam current $\sim$10 mA, range from $\phi_0\sim10^3$ V for an unscreened beam to

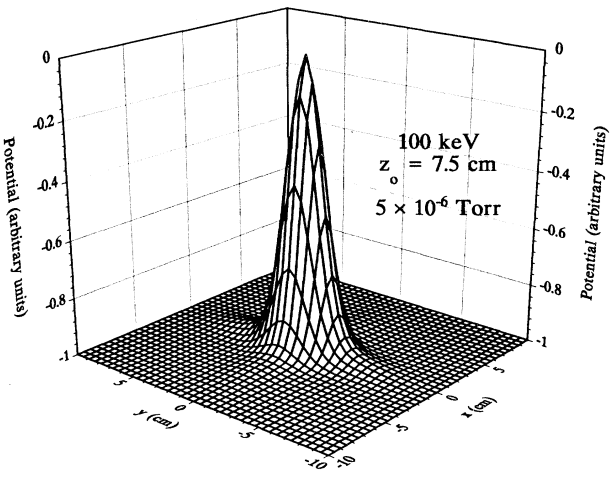

FIG. 9. Beam potential for a 100 keV, 10 mA arsenic beam propagating through a chamber at 5×10^{-6} Torr. Although the beam possesses a 2:1 aspect ratio, the potential displays a high degree of cylindrical symmetry.

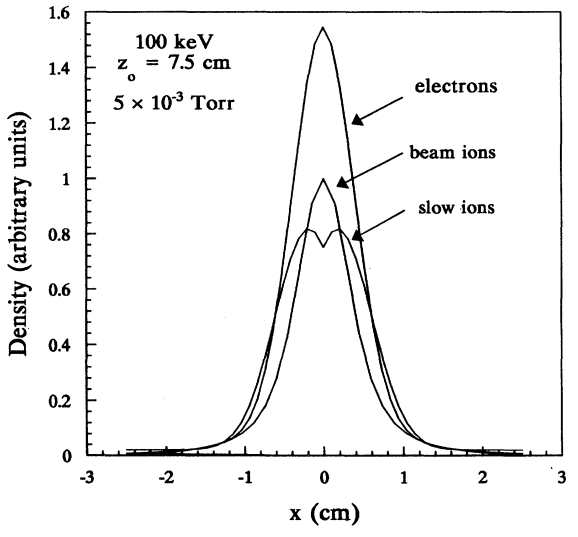

FIG. 11. Beam ion, slow-ion, and electron densities for a 100 keV, 10 mA arsenic beam propagating through a chamber at 5×10^{-3} Torr. At this pressure the electron and slow-ion densities are significantly larger than in Fig. 8 and the beam is fully neutralized along the axis.

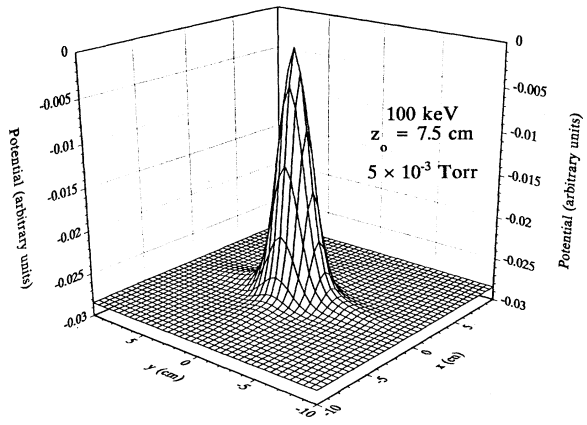

FIG. 12. Potential for a 100 keV, 10 mA arsenic beam in a chamber at 5×10^{-3} Torr. The axial potential is two orders of magnitude less than that of Fig. 9.

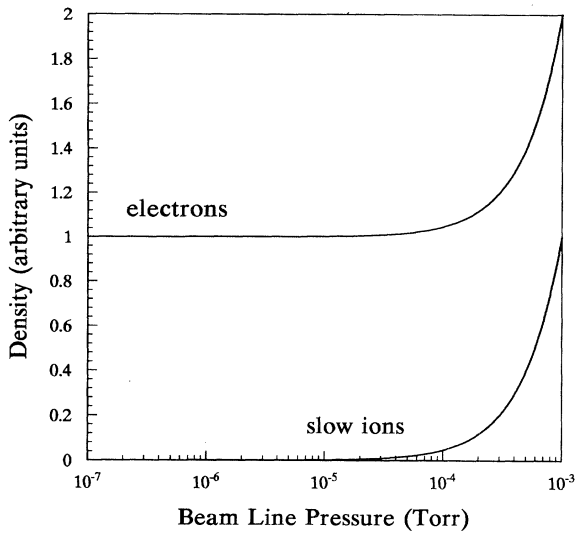

FIG. 13. Variation of the axial electron and slow-ion densities with chamber pressure [Eqs. (8) and (18)] under the assumption of axial charge neutrality.

$\phi_0 \sim 10-10^2$ V for the beam plasma.)

Increasing the beamline pressure increases the scattering rate and enhances the production of electrons and slow ions. Normalized to an axial beam ion density of unity, the carrier densities characterizing the 100 keV, 10 mA arsenic beam propagating through a beam line with a residual gas pressure of 5×10^{-3} Torr differ dramatically from the low pressure calculation. In Fig. 11, the electron density possesses a maximum approximately 1.6 times that of the beam ions, while the slow-ion density is nearly comparable to that of the beam ions. Again, the axial densities were determined self-consistently. In this case, however, the condition of axial charge neutrality is satisfied by the greater electron creation rate, and the beam is more fully neutralized. The potential profile of Fig. 12, normalized to that of Fig. 9, essentially retains the previous shape, but with a beam potential ϕ_0 nearly two orders of magnitude below that of the low pressure value. Variations of the electrons and slow-ion densities with beam line pressure, as calculated from Eqs. (8), (18), and the ideal gas law, are presented in Fig. 13. The functional dependence of the slow-ion density on beam ion concentration is plotted in Fig. 14, while Fig. 15 shows that increasing the residual gas pressure within the beamline diminishes the beam potential, which, in some applications such as ion implantation, could help reduce the entrainment of contaminating particles, but at the expense of optimal beam propagation and performance.

In general, the preceding analysis does not predict complete neutralization. It is, therefore, expected that the beam will continue to evolve into a cylindrically symmetric configuration of minimum self potential energy. Neglecting ion-gas collisions, an estimate of the distance required for the beam to transform from a high aspect ratio rectangle to a cylindrical Gaussian can be gleaned from the ion density profile of Eq. (25). The condition for the cosine series to approximate a Gaussian surface is $\alpha_n x \ll 1$ and $\beta_m y \ll 1$. Invoking this condition introduces the constraints $2n+1 \ll 4L_x/\pi w$ and $2m+1 \ll 4L_y/\pi h$, producing the value $\gamma = 2\sqrt{w^{-2}+h^{-2}}$. These constraints will be satisfied when $\gamma^2 \exp(-\gamma z/\eta) \ll 1$. Solving for z, the axial distance at which the beam can be expected to lose its well-defined aspect ratio is

$$z \cong h\eta \ln(2\sqrt{w^{-2}+h^{-2}})/\sqrt{w^{-2}+h^{-2}} \ .$$

For a 100 keV beam emanating from 1 eV source, $z \sim 2$ m.

Finally, in repeating the numerical analysis for a 100 keV, 10 mA arsenic beam of unit aspect ratio, the results

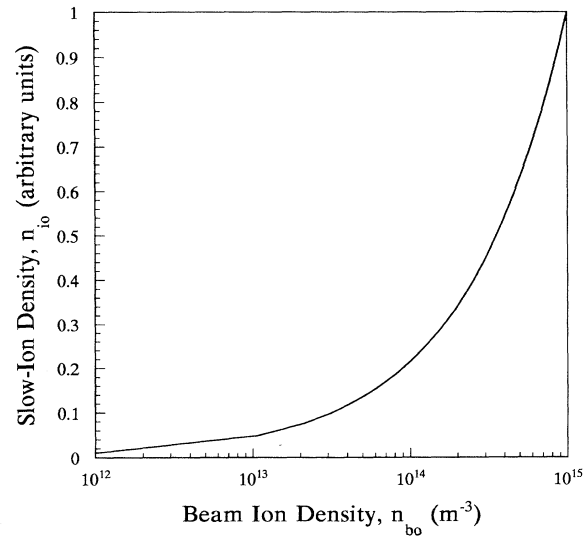

FIG. 14. Variation of the axial slow-ion density with the axial beam ion density at fixed pressure [using Eq. (C9) with ϕ_0 from Eq. (24)].

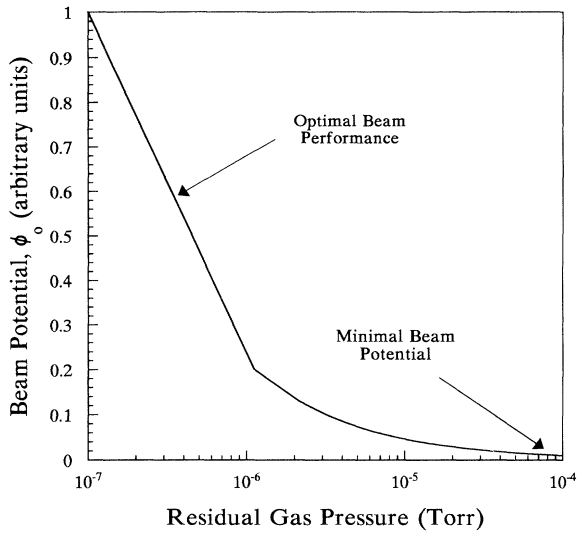

FIG. 15. Beam potential ϕ_0 as a function of chamber pressure [from Eq. (24)].

of Figs. 6 and 8–12 were recovered, with the x and y cross sections now being identical. Comparison of the curves appearing in Figs. 8 and 11 to results reported by Holmes [6] reveals the square beam profiles to be in good agreement with predictions for a cylindrical beam.

V. CONCLUSION

A complete, self-consistent two-dimensional description of an intense rectangular ion beam with space-charge neutralization has been presented. Calculations predict the electrostatic potential and corresponding electric fields to possess a remarkable degree of cylindrical symmetry, irrespective of the aspect ratio of the beam ion density, a result which has been observed experimentally [9]. Moreover, in concert with previous work [1], this analysis demonstrates that cylindrically symmetric potentials may be appropriately applied to approximate beams of differing geometry. In particular, this work serves to help define the domain of validity for the copious works currently in the literature that are based upon *a priori* assumptions of a Gaussian profile. Thus many beam properties related to space-charge effects, including the conditions for entrapment and transport of particulate contamination [9–12], remain essentially the same for beams of varying cross-sectional configurations.

ACKNOWLEDGMENTS

This work was supported by the Arizona SEMATECH Center of Excellence and by IBM.

APPENDIX A: ELECTRON RELAXATION TIME

The low-energy perturbation to the electron energy distribution function arises during the transient evolution of the electron cloud, from its creation, to the establishment of the steady state. After extinction of the transients, the perturbation maintains a time invariant number density with a magnitude that is dependent on the electron creation rate, and the time necessary for the system to relax into the steady state. Spitzer [7] has estimated the time for an anisotropic energy distribution in a self-interacting electron gas of density n_e to approach an isotropic Maxwellian distribution. Denoting this time δt, his estimate is given in terms of the number density n_e by

$$\delta t = 0.266 \frac{T^{3/2}}{n_e \ln\Lambda} , \tag{A1}$$

where δt is in seconds and T is in kelvin. The value of $\ln\Lambda$ depends on the electron temperature and density, but is normally assumed to have a value of approximately 10 [7].

For an order of magnitude estimate, suppose the electron gas engulfing the beam possessed a rather high temperature of 100 eV, corresponding to about 1.2×10^6 K. The numerator would then be on the order of 10^8, and the relaxation time would scale as

$$\delta t \sim \frac{10^7}{n_e} . \tag{A2}$$

APPENDIX B: INTEGRATION OF THE TRUNCATED DISTRIBUTION

The finite depth of the positive potential well precludes the complete confinement of thermalized electrons. Electrons possessing kinetic energies in excess of the beam potential cannot exist within the distribution. If the system is essentially Maxwellian, the finite beam potential leads to a renormalization of the distribution function. This renormalization produces the general expression

$$f(v) = \frac{\int_0^v e^{-mv'^2/2kT} d^3v'}{\int_0^{v_{\max}} e^{-mv'^2/2kT} d^3v'} .$$

For an isotropic distribution, the integrand is most conveniently expressed in spherical coordinates. The numerator and denominator then assume the identical form

$$\int_0^v e^{-mv'^2/2kT} d^3v' = 4\pi \int_0^v e^{-mv'^2/2kT} v'^2 dv' .$$

Letting $u = v'\sqrt{m/2kT}$, the integrand is converted to a dimensionless variable and the integral becomes

$$4\pi \int_0^v e^{-mv'^2/2kT} v'^2 dv' = 4\pi \left[\frac{2kT}{m}\right]^{3/2} \int_0^{\sqrt{mv^2/2kT}} u^2 e^{-u^2} du .$$

Arranging the differential term as $u\exp(-u^2)du$ or $\exp(-u^2)du$ permits integration by parts in two different ways, producing two equivalent but functionally different results:

$$\int_0^{\sqrt{a}} u^2 e^{-u^2} = \begin{cases} -\dfrac{e^{-a}\sqrt{a}}{2} + \dfrac{\sqrt{\pi}\,\mathrm{erf}(\sqrt{a})}{4} \\ \dfrac{\sqrt{\pi}}{2}\left[a\,\mathrm{erf}(\sqrt{a}) - 2\int_0^{\sqrt{a}} \mathrm{erf}(u)u\,du\right], \end{cases} \tag{B1}$$

where

$$\mathrm{erf}(x) = \frac{2}{\sqrt{\pi}} \int_0^x e^{-u^2} du$$

is the error function.

APPENDIX C: SLOW-ION AXIAL DENSITY AND THE ELECTROSTATIC POTENTIAL

From Ref. [1], it is known that in the limit of vanishing x and y the beam ion density is nearly cylindrically symmetric. This fact will be exploited to determine the slow-ion density and the profile of the electrostatic potential along the beam axis.

In any cylindrical volume coaxial with the beam, slow ions created at some radius ρ contribute to the flux at some further radius r. Expressing the differential form of the continuity equation in cylindrical coordinates, the requirement of charge conservation may be written

$$dn_i(r) v r\, d\theta\, dz = n n_b(\rho) v_b \sigma_t (\rho\, d\rho) d\theta\, dz\ . \tag{C1}$$

With $v = \sqrt{2q[\phi(\rho) - \phi(r)]/m_i}$, solving for $dn_i(r)$ and integrating produces an expression for the slow-ion density valid for small r:

$$n_i(r) = \left[n v_b \sigma_t \left[\frac{m_i}{2q} \right]^{1/2} \right] \frac{1}{r} \int_0^r \frac{n_b(\rho)\rho\, d\rho}{\sqrt{\phi(\rho) - \phi(r)}}\ . \tag{C2}$$

In the limit $r \to 0, n_b(\rho) \approx n_b(r) \approx n_{b0}$, and the integral may be slightly simplified:

$$n_i(r) = \left[n n_{b0} v_b \sigma_t \left[\frac{m_i}{2q} \right]^{1/2} \right] \frac{1}{r} \int_0^r \frac{\rho\, d\rho}{\sqrt{\phi(\rho) - \phi(r)}}\ . \tag{C3}$$

From the continuous charge distribution and the beamline geometry, the potential must be continuous, finite, and monotonic. It is therefore permissible to expand the potential in a Maclaurin series,

$$\phi(r) = 0 + \phi_1 \frac{r}{r_0} + \phi_2 \left[\frac{r}{r_0} \right]^2 + \phi_3 \left[\frac{r}{r_0} \right]^3 + \cdots\ . \tag{C4}$$

Here, the first term is zero by definition, r_0 is a characteristic length scale, and ϕ_i are the coefficients of expansion.

Suppose the first nonvanishing term in the series is of order m. A Maclaurin series for a continuous, finite, monotonic function is absolutely covergent. Thus, for small r, the first nonvanishing term will also be the dominant term,

$$\phi(r) \approx \phi_m \left[\frac{r}{r_0} \right]^m\ . \tag{C5}$$

The slow-ion density now assumes the form

$$n_i(r) \approx \left[n n_{b0} v_b \sigma_t \left[\frac{m_i}{2q\phi_m} \right]^{1/2} \right] r_0^{m/2} \times \frac{1}{r^{1+m/2}} \int_0^r \frac{\rho\, d\rho}{\sqrt{1 - (\rho/r)^m}}\ . \tag{C6}$$

Letting $u = (\rho/r)^m$, the integrand is converted to a dimensionless variable. After simplification, the explicit r dependence is removed from the integrand and appears as a prefactor:

$$n_i(r) = \left[n n_{b0} v_b \sigma_t \left[\frac{m_i}{2q\phi_m} \right]^{1/2} \right] r_0^{m/2} \times r^{1-m/2} \int_0^1 \frac{u^{-(m-2/m)} du}{\sqrt{1-u}}\ . \tag{C7}$$

The integral is now independent of r, and finite for all m. Axial behavior of the function is solely determined by the r dependence of the prefactor. By inspection, if $m > 2$, n_i diverges as r tends to zero. Conversely, if $m < 2$, the density vanishes for vanishing r. Only for $m = 2$ is the density finite and consistent with the physical situation. For $m = 2$,

$$\int_0^1 \frac{du}{\sqrt{1-u}} = 2$$

and

$$n_{i0} = \left[n n_{b0} v_b \sigma_t \left[\frac{m_i}{2q\phi_2} \right]^{1/2} \right] r_0\ . \tag{C8}$$

In Sec. II C, Eq. (22), it is shown that if $\phi_2 = \beta^2 \phi_0$ then $\beta^2 = \frac{1}{3}$. The axial value of the slow-ion density then becomes

$$n_{i0} = \left[n n_{b0} v_b \sigma_t \left[\frac{3m_i}{2q\phi_0} \right]^{1/2} \right] r_0\ . \tag{C9}$$

[1] D. Brown and J. O'Hanlon, Phys. Rev. E **48**, 523 (1993).

[2] D. Brown, Ph.D. dissertation, Department of Electrical and Computer Engineering, University of Arizona, Tucson, Arizona, 1992.

[3] M. E. Rudd and T. Jorgensen, Phys. Rev. **131**, 666 (1963).

[4] M. Gryzinski, Phys. Rev. **115**, 374 (1959).

[5] M. N. Rosenbluth, W. M. MacDonald, and David L. Judd, Phys. Rev. **107**, 1 (1957).

[6] A. J. T. Holmes, Phys. Rev. A **19**, 389 (1979).

[7] Lyman Spitzer, *Physics of Fully Ionized Gases,* 2nd ed. (Wiley, New York, 1962).

[8] Earle H. Kennard, *Kinetic Theory of Gases* (McGraw-Hill,

New York, 1938).
[9] D. Brown, P. Sferlazzo, S. Beck, and J. O'Hanlon, J. Appl. Phys. **71**, 2937 (1992).
[10] D. Brown, P. Sferlazzo, and J. O'Hanlon, *Proceedings of the 36th Institute of Environmental Sciences Technical Meeting* (IES, Mt. Prospect, Il, 1990), pp. 396–400.
[11] D. Brown, P. Sferlazzo, and J. O'Hanlon, Nucl. Instrum. Methods Phys. Res. Sect. B **55**, 348 (1991).
[12] D. Brown, P. Sferlazzo, and J. O'Hanlon, J. Am. Vac. Sci. A **9**, 2808 (1991).